Desalination 604 (2025) 118669

Contents lists available at ScienceDirect

Desalination

journal homepage: www.elsevier.com/locate/desal

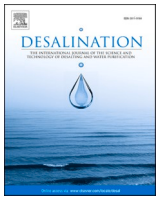

Enhancing hydrophilicity of thick electrodes via sulfonation reaction for lithium extraction from salt lake

Junyi Zhang [a], Luxiang Ma [a,*], Chunxi Hai [a], Tiandong Chen [a], Yawen Gao [a], You Xu [a], Wencheng Pan [a], Ju Chen [a], Yanxia Sun [a], Shengde Dong [a], Xin He [a], Qi Xu [a], Xiaowang Wu [c], Caixiong Quan [c], Hongli Su [b,*], Yuan Zhou [a,*]

[a] College of Materials and Chemistry & Chemical Engineering, Cheng Du University of Technology, Cheng Du 610059, PR China
[b] Resource & Recycling, Department of Engineering Structures, Faculty of Civil Engineering and Geosciences, Delft University of Technology, Delft 2628 CN, the Netherlands
[c] Qinghai Zhongxin Guoan Lithium Development Co., LTD., Qinghai Key Laboratory of Comprehensive Utilization of Sulfate Salt Lake Resources, Ge Er Mu 816000, PR China

HIGHLIGHTS

- The S-PVDF thick electrode effectively enhances the mass transfer between the thick electrode and the brine.
- The practicability of hydrophilic thick electrode for extracting lithium from actual brine was confirmed.
- The hydrophilic thick electrode prepared by simple sulfonation process highlights its potential for application.

ARTICLE INFO

Keywords:
Lithium extraction from Salt Lake
Electrochemical de-lithiation method
Sulfonation reaction
Thick electrode
Hydrophilic

ABSTRACT

Thick electrodes greatly enhance lithium extraction capacity. However, with the increase of active substances loading, the traditional thick electrodes are more hydrophobic, severely limiting the utilization of active substances. Hence, a sulfonation process to functionalize thick electrodes was applied to enhance their wettability (~45 $mg{\cdot}cm^{-1}$) in brine. Experimental and theoretical results show that the lithium extraction capacity of thick electrodes can be significantly improved by enhancing the electrodes hydrophilicity. At 0.8 V, the S-PVDF electrode's capacity for lithium extraction in simulated brine (41.72 $mg{\cdot}g^{-1}$) significantly surpassed the PVDF electrode (35.72 $mg{\cdot}g^{-1}$), and it also performed well in actual brine (28.8 $mg{\cdot}g^{-1}$). The Mg^{2+}/Li^{+} ratio in actual brine dropped from 65 to 0.37, achieving effective magnesia-lithium separation. This method offers a novel approach to developing high-efficiency lithium extraction thick electrodes.

1. Introduction

The rapid growth of the lithium-ion battery industry has generated a substantial demand for efficient extraction lithium technology [1–3]. Lithium extraction from salt lakes stands out among various lithium resources due to its economic, environmentally friendly, and adaptable nature [4]. Electrochemical de-lithiation extraction technology offers distinct advantages, including low cost and wide applicability, making it a widely accepted solution for large-scale lithium extraction in both academia and industry [5–7]. Electrochemical lithium extraction system operates similarly to a lithium-ion battery, using electrode materials, supporting electrolyte, brine, and anionic film. The anode employs Li-rich lithium material, while the cathode uses sub-stoichiometric lithium material. Li^{+} are selectively extracted from the brine, facilitating the separation and extraction of Li^{+} [8]. For instance, Zhao et al. [9] A novel lithium extraction system was developed, comprising $LiMn_2O_4$ (anode), a supporting electrolyte, an anionic membrane, brine, and $Li_{1-x}Mn_2O_4$ (cathode), tailored for brine with low Li^{+} concentrations. This system reduced the Mg^{2+}/Li^{+} ratio from 147.8 in the brine to 0.37 in the cathodic solution, while increasing the Li^{+} concentration in the supporting electrolyte to 1.2 $g{\cdot}L^{-1}$. Additionally, Zhao et al. [10] confirmed that LFP materials effectively achieve Mg/Li separation,

* Corresponding authors.
E-mail addresses: maluxiang@cdut.edu.cn (L. Ma), h.su-3@tudelft.nl (H. Su), zhouy@cdut.edu.cn (Y. Zhou).

https://doi.org/10.1016/j.desal.2025.118669
Received 26 August 2024; Received in revised form 23 December 2024; Accepted 6 February 2025
Available online 9 February 2025

reducing the Mg/Li ratio from 60 to 0.45. Meanwhile, The research group [11] found that $Li_{0.3}FP$ materials exhibit higher ion selectivity for Na compared to FP. Their results indicate that achieving a Li/Na separation coefficient of 138 reduces the Na/Li mass ratio in brine from 184 to 1.33. This research has greatly contributed to improving the selectivity of active materials and adaptability to various brines. However, low yield and efficiency in lithium extraction remain significant challenges, limiting the widespread practical use of the electrochemical de-lithiation method.

Large size, high load thick electrode is the key to solve this issue. However, the increased thickness of the electrode brings challenges to the wettability of the electrode sheet in brine. For aqueous batteries, the wettability of high-load electrode and electrolyte has been extensively studied. Lee et al. [12] employed a straightforward sulfonation process to create a hydrophilic thick electrode (~6 $mg{\cdot}cm^{-2}$), enhancing the battery's overall energy density. However, salt lake brine exhibits high calcification and viscosity. Its unique chemical properties will put higher demands on electrode construction. Moreover, increased electrode thickness hinders full impregnation of the electrode sheet with brine, directly raising transfer resistance at the solid-liquid interface and reducing the electrochemical surface's effectiveness [13]. The electrode material near the fluid collection point cannot fully exert its de-lithiation effect, leading to lower lithium extraction efficiency. Thus, improving the wettability of thick electrodes is crucial to overcoming the low yield and efficiency in electrochemical de-lithiation.

In this study, PVDF (S-PVDF) was functionalized through a straightforward process to construct a high-load thick electrode (45 $mg{\cdot}cm^{-2}$). This enhancement improved the electrode's wettability in salt lake brine, thereby enhancing the lithium extraction efficiency of the electrode. S-PVDF thick electrode can effectively enhance lithium extraction capacity compared to traditional PVDF, while maintaining adhesion. The binding capacity of S-PVDF and PVDF thick electrode was equivalent (0.815 N Vs. 0.814 N). Additionally, the S-PVDF electrode also showed a high intercalating capacity of 28.8 $mg{\cdot}g^{-1}$ in actual brine. It provides valuable guidance for the future industrial application of electrochemical de-lithiation methods.

2. Materials and methods

2.1. Reagents

N-methyl-2-pyrrolidinone (NMP, ≥99.0 %), acetylene black (C, ≥99 %), and PVDF (≥99.0 %) were all purchased from the Chengdu Colon Chemical Co., LTD. Potassium chloride (KCl, 99.0 %), Lithium chloride (LiCl, ≥99.0 %), Sodium chloride (NaCl, ≥99.0 %), Magnesium chloride hexahydrate ($MgCl_2$, ≥99.0 %) Lithium iron phosphate ($LiFePO_4$), Chlorosulfonic acid (Cl-SO_2OH) and 1,2-dichloroethane were all obtained from the Beijing inoke Co., Ltd.

2.2. Synthesis of S-PVDF binders

S-PVDF synthesis, detailed in **Fig. S1**, involves dissolving 2 g of PVDF powder in 20 mL of Cl-SO2OH within a 50 mL vial, followed by heating at 80 °C with constant stirring for 30 min. The solution is then precipitated in 1,2-dichloroethane and washed several times with deionized water to achieve a neutral pH of 7. The final step involves vacuum drying at 60 °C for 24 h to produce S-PVDF.

2.3. Preparation of LFP/FP electrode

LFP, S-PVDF/PVDF, and Super P were weighed in a mass ratio of 8:1:1. Initially, S-PVDF/PVDF was dissolved in NMP by thorough stirring at normal temperature (The ratio of adhesive to NMP is 25). Subsequently, lithium iron phosphate and Super P were added and mixed until uniformly blended. The resulting slurry was coated evenly onto a graphite sheet collector at a density of 45 $mg{\cdot}cm^{-2}$ (MSK-AFA-ES200 plate coater was applied at room temperature at a speed of 3.2 cm/s and a pressure of 6Mpa). The coated electrode was dried in an air-drying oven at 80 °C for 10 h. Following drying, the LFP electrode underwent Li^+ de-intercalation at a constant voltage of 0.8 V to obtain the FP electrode, using a 0.1 M NaCl electrolyte. Additionally, during electrochemical testing and lithium extraction, the pole sheet needs to be activated, and the pole sheet can be immersed in a 0.5 M NaCl solution for 0.5 h–1 h.

2.4. Characterization

The hydrogen environment of the materials was characterized by nuclear magnetic resonance (^{1}H NMR, Bruker 400 MHz, Germany). These materials were analyzed by scanning electron microscopy (SEM Hitachi S-4800), nuclear magnetic resonance spectroscopy (NMR Bruker AVANCEIII 400M), X-ray photoelectron spectroscopy (XPS Thermo ESCALAB) 250XI), Fourier transform infrared absorption spectrometer (FTIR BRUKER TENSOR II) and Transmission electron microscope (TEM FEI-TALOS-F200X) were used to characterize the morphology and structure. The ion content was determined by inductively coupled plasma (ICP-OES AGILENT 730). The electrochemical data were characterized by both the Blue electric system and the Electrochemical workstation (Princeton PARSTAT 4000).

2.5. Electrochemical test method

2.5.1. Charge and discharge test

The electrochemical properties of the prepared materials were evaluated using a LAND test system. The test voltage range was −0.3 V to 0.7 V vs. Hg/HgCl. Long-term cycling was conducted at a current density of 0.2C, and rate capability tests were performed at current densities of 0.1C, 0.2C, and 0.5C. All tests were performed with 0.1 M LiCl solution.

2.5.2. Cyclic voltammetry and AC impedance test

Both cyclic voltammetry (CV) and AC impedance spectroscopy (EIS) tests were conducted using an AUTOLAB workstation. The CV test employed a sweep speed of 0.2 $mV{\cdot}s^{-1}$ over a range from −1 V (with a 0.5 M LiCl solution as the electrolyte). For EIS, the AC frequency range spanned from 100 kHz to 10 mHz, using a perturbation signal of 5 mV (with a 0.5 M LiCl solution as the electrolyte).

2.5.3. Lithium extraction test

Cyclic experiments were conducted using an LFP electrode as the anode in different brine compositions. Electrolysis was performed at a current density of 0.2C until the cell voltage reached 0.3 V, followed by constant voltage electrolysis at 0.3 V until the current density dropped below a cutoff of 20 μA. After each electrolysis cycle, the electrode polarity was reversed to start the next de-intercalation cycle. The pure lithium recycling solution had a NaCl concentration of 0.1 M, while the brine recycling solution had a concentration of 3.5 M NaCl.

2.6. FEA simulation

Finite element method (FEM) was employed for the numerical simulation of water saturation in the thick electrode. Two modules in COMSOL Multiphysics 5.5 were used, including Darcy's law and phase transfer in porous media modules [14–16]. The solution was absorbed in the thick electrode due to the hydrophilicity of the thick electrode, and the solution flowed in the nano porous structure of the thick electrode. The phase transfer in porous media module was used to simulate multiphase flow in porous media with two moving phases (e.g., brine and air), and determined the density changes of the liquid phase. The Darcy's law module was used to describe the solution flow (velocity) driven by the hydrophilicity of the thick electrode. The applied non-flux boundary conditions were set at the solid-fluid interface in the phase

transfer in porous media and Darcy's law modules. In addition, the outlet pressure was adjusted by multiple factors (e.g., hydrophilicity of the thick electrode). The employed parameters were shown in Table S1.

3. Results and discussion

3.1. Morphology and structure of S-PVDF and PVDF electrodes

Fig. 1a illustrates the prepared S-PVDF and pristine PVDF. Additionally, the LFP particles exhibit uniform size, primarily around 200 nm (Fig. 1b). Fig. 1c and d depicts the plane and cross-sectional views of the thick electrode (~45 mg·cm^{-2}) prepared by blending with PVDF and S-PVDF. It can be seen that the flat particles are relatively uniform with a thickness of approximately 451.9 μm.

EDS analysis, shown in Fig. 1e, revealed the presence of S and F elements with a uniform distribution across the analyzed area. Fig. 1f indicates that the particle surfaces are uniformly coated with a layer of S-PVDF. Additionally, Fig. 1g shows 211 crystal facets on LFP, covered by a layer of amorphous material. Notably, the structure of LFP particles remained unchanged after treatment with both PVDF and S-PVDF (Fig. S2a and b).

3.2. Structure of S-PVDF and PVDF

XPS images clearly indicate the successful introduction of sulfonic functional groups. XPS spectra before and after sulfonation are presented in Figs. 2 and S3, revealing the presence of F1s(685 eV), O1s(530 eV), C1s(283 eV), and S2p(167 eV) in S-PVDF. The detection of S suggests successful incorporation of sulfonic functional groups (Fig. S3). Fig. 2a and b shows the fine spectrum of C1s of the two materials, where the bond energies of C—F, C-S/C=O, -CH_2-CF_2-, and C=C are 289 eV, 286.4 eV, 284.6 eV, and 283.1 eV respectively [17–19]. Sulfonation of PVDF significantly reduces the relative content of C—F and -CH_2-CF_2- bonds, indicating the substitution of F atoms with sulfonic groups, confirming the successful introduction of these functional groups. Additionally, the increase in C=C bonds after sulfonation may result from a few side reactions [20]. The C=C bond was also found in FTIR spectra at wavelength 1563 cm^{-1} (Fig. 2e) [21]. Furthermore, sulfonic functional groups were detected in the fine S2p spectrum (Fig. 2c), with no signal of PVDF observed (Fig. S4), further corroborating the successful grafting of sulfonic functional groups [22].

The ^{1}H NMR spectroscopy confirmed PVDF's sulfonation, evidenced by two peaks at 3.0–3.1 and 2.3–2.4 ppm, indicating head-to-tail and head-to-head bonds in semi-crystalline PVDF (HA,A′), respectively (Fig. 2d) [23]. A shift to lower chemical shifts (6.2–6.5 ppm) is attributed to hydrogen bonded to sulfonated carbon. FTIR spectroscopy was confirmed the presence of functional groups, particularly sulfonic acid, on the polymer chains. Fig. 2e compares the FTIR spectra of pure PVDF and S-PVDF, showing a peak at ~1045 cm^{-1} corresponding to the symmetric stretching vibrations of aromatic sulfonic acid. The asymmetrical stretching vibrations of sulfonic groups are marked by a peak around 1192 cm^{-1}. However, identifying this peak in the FT-IR spectrum is challenging due to overlap with absorption from the predominant PVDF groups at the same wavelength [24]. This overlap indicates the incorporation of sulfonic functional groups into the polymer chains.

3.3. Electrochemical performance

Fig. 3a illustrates the discharge/charge curve at a 0.2C rate. Using PVDF as an adhesive, the thin electrode achieved a high specific capacity of 163.5 mAh·g^{-1}. In contrast, the thick electrode's capacity was limited to 124.3 mAh·g^{-1}, indicating a constraint in the capacity of electrodes with PVDF binder when they are thick. Notably, the capacity significantly improved for the thick electrode when using an S-PVDF binder, reaching nearly 163.4 mAh·g^{-1}, this marks a remarkable enhancement compared to the standard PVDF binder at the same level of active mass loading. This demonstrates that the sulfonated binder enhances the permeability of the high-loaded electrode to brine, improves the utilization of the active material, and increases the mass transfer rate of Li^+ in brine, closely linked to the sulfonic functional group in PVDF. Similarly, electrodes with S-PVDF binder show higher capacity in cycling and rate performance. The overall capacity of the S-PVDF electrodes was higher than that of PVDF at 0.2C (Fig. 3c). Additionally, the capacity retention rate of S-PVDF electrode after 50 cycles (76 %) was higher than that of PVDF electrode (55.5 %). Cycling tests at different current densities showed that the capacity of the S-PVDF electrode consistently exceeded that of the PVDF electrode (Fig. 3b). Additionally, as shown in the CV curve (Fig. 3d), the peak voltage difference for the PVDF

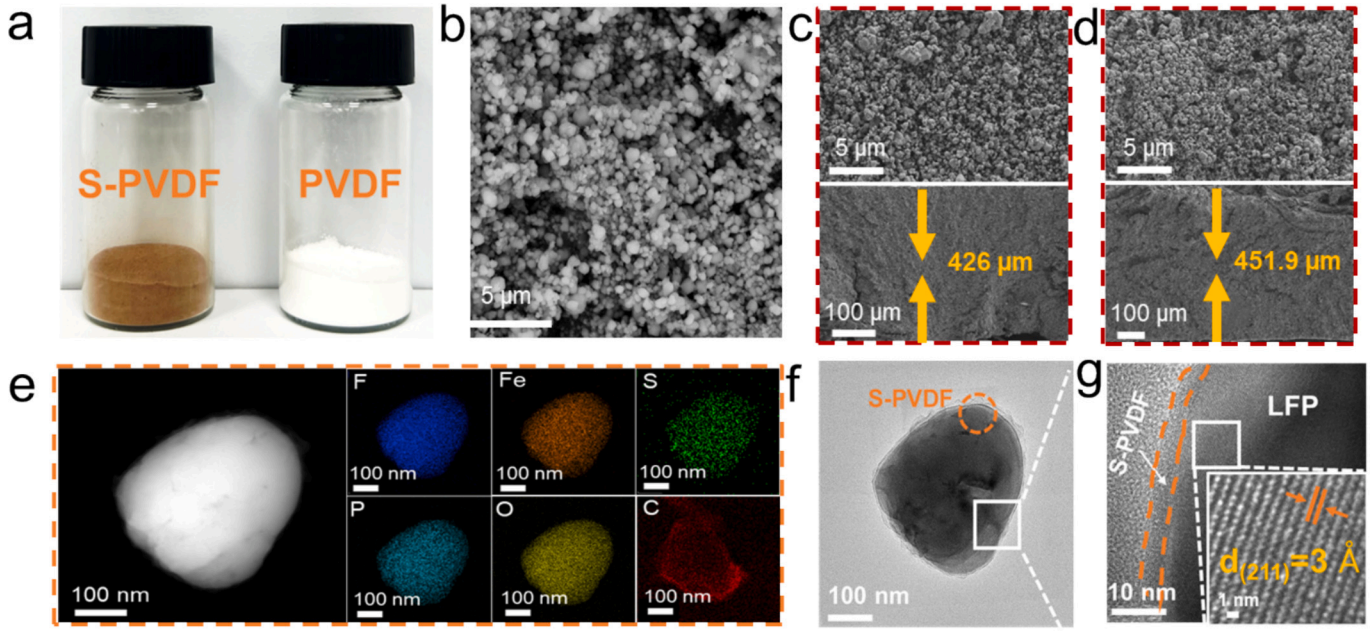

Fig. 1. Morphology and structure of S-PVDF and PVDF electrodes. (a) Physical drawings of S-PVDF and PVDF. (b) FE-SEM image of LFP. (c) FE-SEM images of PVDF and (d) S-PVDF thick electrode planes and cross sections. (e–g) HAADF-STEM images and (e) EDS images of S-PVDF electrode.

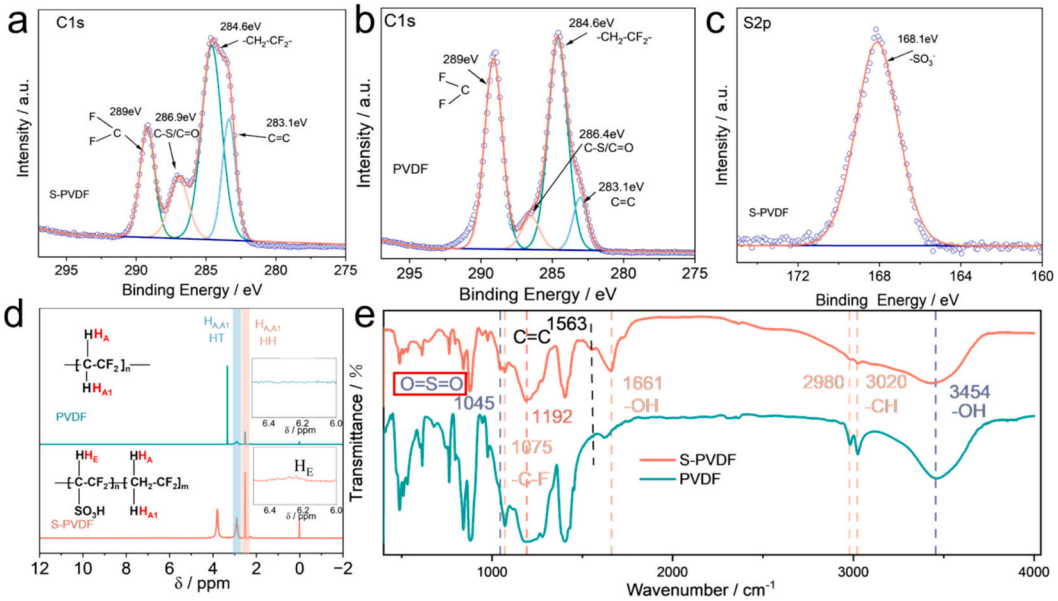

Fig. 2. Structure of S-PVDF and PVDF. (a) High resolution spectra of C1s for S-PVDF. and (b) C1s for PVDF. (c) S2p for S-PVDF. (d) ^{1}H NMR spectra of S-PVDF and PVDF binders. (e) FT-IR spectra of S-PVDF and PVDF binders.

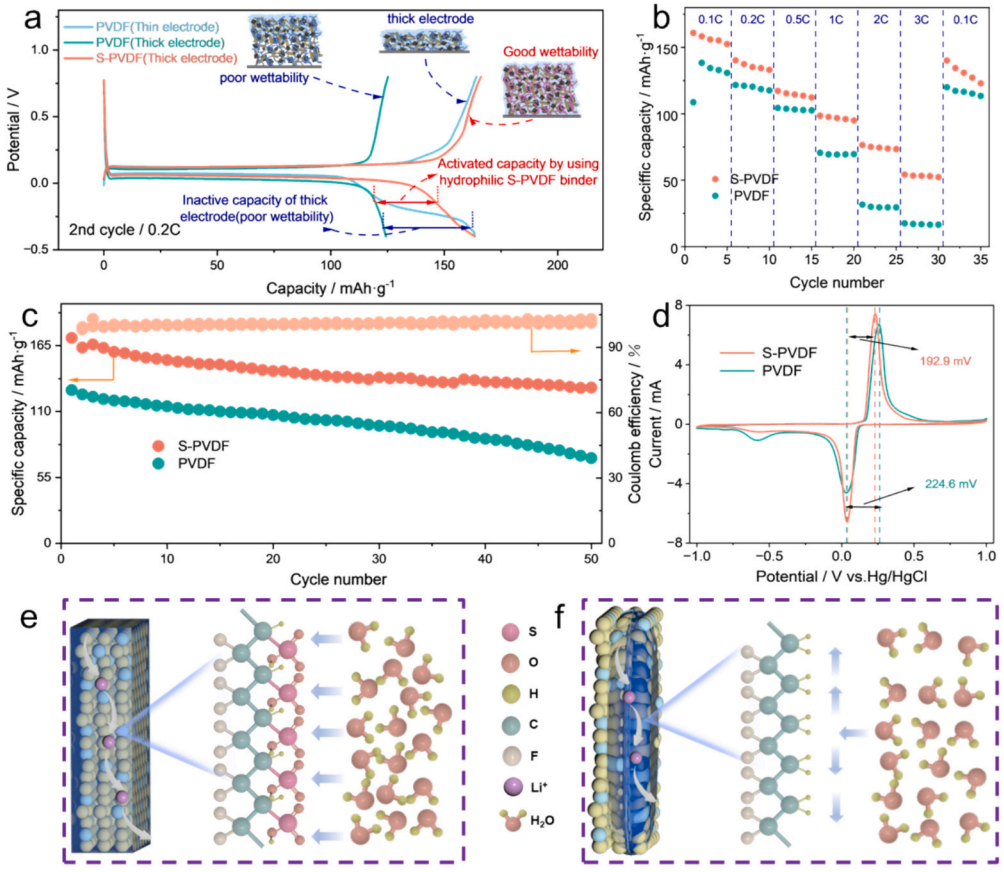

Fig. 3. Electrochemical properties of two binders. (a) Charge and discharge curves of thick and thin electrodes under different binders (the 2nd cycle). (b) Specific discharge capacity of S-PVDF binder at different multipliers. (c) Cycling performance of PVDF and S-PVDF thick electrode at 0.2C. (d) CV curve at 0.2 mV·s^{-1}. (e) Hydrophilic diagram of S-PVDF. (f) PVDF hydrophobic diagram.

electrode (224.6 mV) was significantly higher than that of the S-PVDF electrode (192.9 mV). This means that S-PVDF electrode has better electrochemical reaction kinetics. Meanwhile, the impedance of S-PVDF electrode (21.1 Ω) was significantly lower than that of PVDF (37.1 Ω) (Fig. S5). The results indicate an enhancement in the kinetics performance of the thick electrode following sulfonation.

To explain the increase in capacity of the S-PVDF electrode from a microscopic perspective (Fig. 3e and f), we examine the hydrophilicity

and hydrophobicity of the two electrodes. The incorporation of sulfonate groups into PVDF's hydrophobic polymer chains creates hydrophilic domains, enhancing its overall hydrophilicity, as depicted in Fig. 3e. This modification, however, leads to incomplete infiltration within PVDF. Moreover, these sulfonate groups act as active sites, modulating ion transfer due to their affinity for Li^+ [25]. The addition of sulfonic acid groups to PVDF improves its brine infiltrability and increases the ion-accessible area. This modification enhances Li^+ transfer, thereby boosting the utilization efficiency of active materials in thick electrodes.

3.4. Lithium extraction performance

The lithium extraction kinetics of thick electrodes with S-PVDF or PVDF were tested to study the impact of hydrophilicity on lithium extraction (Fig. 4a). Both electrodes reach saturation in Li^+ capacity at around 60 min. The S-PVDF electrode achieves a capacity of 41.72 $mg{\cdot}g^{-1}$ (94.8 %), while the PVDF electrode reaches only 35.72 $mg{\cdot}g^{-1}$ (81.2 %). These results indicate that the hydrophilicity of the electrode affects Li^+ capacity, aligning with the electrochemical performance findings. Additionally, the S-PVDF electrode exhibits a higher capacity for two reasons: 1) The S-PVDF thick electrode was tested in a high-concentration pure Li^+ solution (4200 ppm Li^+), ensuring the LFP particles' surface remains rich in Li^+ without interference from impurity ions, thus preventing concentration polarization. 2) The introduction of sulfonic acid improves the wettability of the brine and thick electrode. In the PVDF electrode, 19 % of the active material remained unused, but with the sulfonate, the utilization rate increased by about 14 %. The hydrophilicity of S-PVDF allows brine to penetrate the electrode more easily, increasing the contact area with LFP and thus enhancing capacity. To assess the adaptability of the S-PVDF electrode to varying Li^+ concentrations, its CV curves and Li^+ intercalation capacity at 100 ppm, 200 ppm, and 500 ppm Li^+ concentrations were tested (Fig. 4b and d). The S-PVDF electrode exhibits an impingement potential at all three low Li^+ concentrations (Fig. 4b), suggesting preliminary adaptability to low Li^+ conditions. The peak area of the CV curve, which reflects the de-intercalation capacity of Li^+, gradually increases with higher Li^+ concentrations. This trend indicates that the electrode may possess a high adsorption capacity at elevated concentrations. Additionally, we quantitatively analyzed the embedding capacity of S-PVDF and PVDF (Fig. 4c). We observed significant differences in the initial and subsequent cyclic Li^+ removal capacities of the electrodes at a 100 ppm Li^+ concentration. The difference in capacity at a 100 ppm Li^+ concentration is due to the newly prepared LFP electrode being Li^+ saturated in the first cycle, whereas subsequent cycles involve Li^+ removal and potential Li^+ vacancies, resulting in lower Li^+ content. Both electrodes demonstrated robust capacities exceeding 200 ppm. This can be attributed to the low Li^+ concentration in the 100 ppm solution, where Li^+

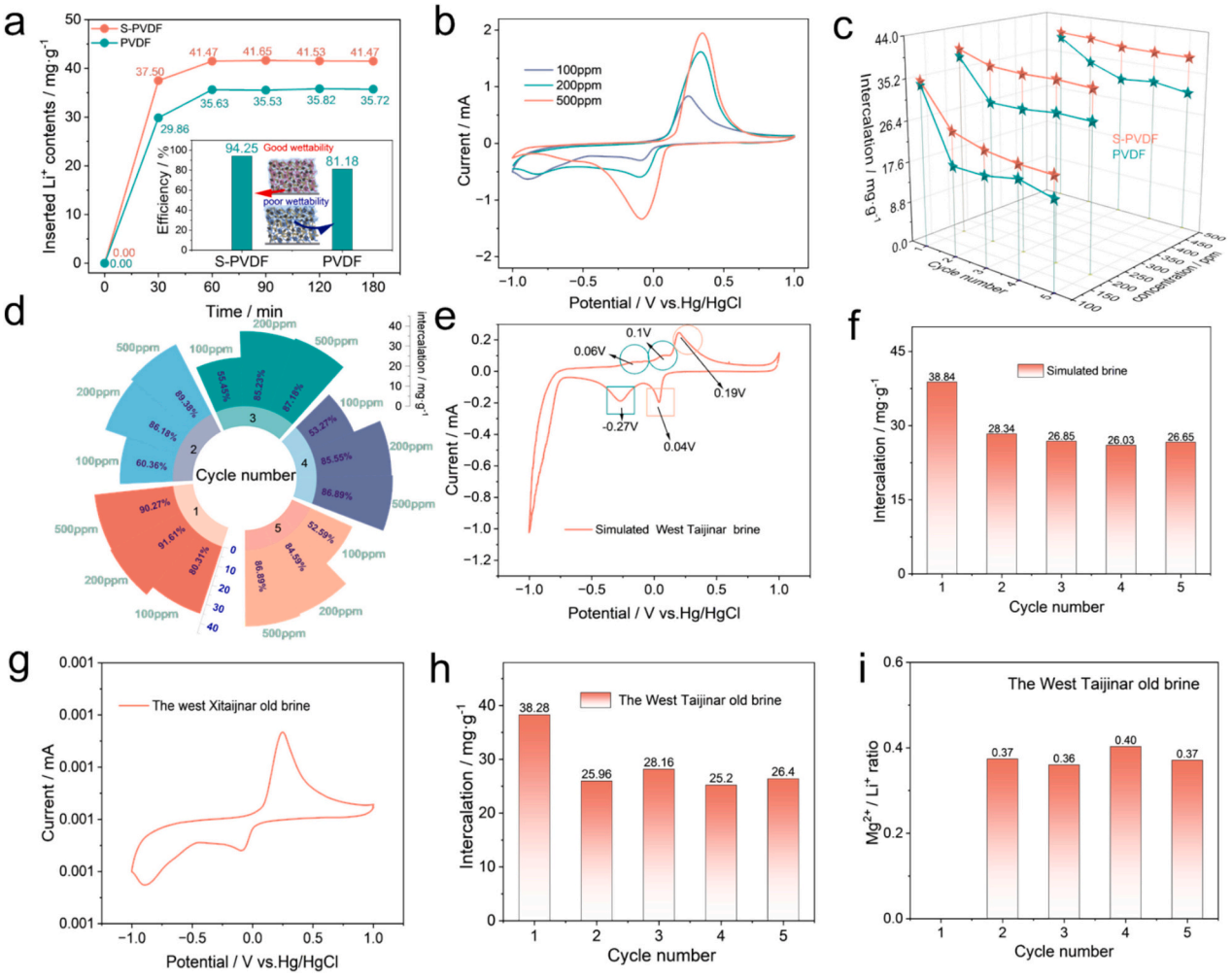

Fig. 4. Lithium extraction performance. (a) Li^+ intercalation capacity as a function of time for both binders. (b) CV curves at different low Li^+ concentrations. (c) Intercalation ability of two electrodes with different Li^+ concentrations. (d) Intercalation efficiency of S-PVDF electrode with different Li^+ concentration. (e) CV curve tested in simulated brine and (f) Li^+ intercalation capacity. (g) CV curve tested in actual old brine. (h) Li^+ intercalation capacity. (i) Change of Mg^{2+}/Li^+ ratio in cyclic extraction of lithium.

uptake in the active material of the thick electrode surpasses the replenishment rate from the solution phase. This mismatch leads to significant concentration polarization, reducing capacity. In contrast, the higher capacities observed at 200 ppm and 500 ppm likely stem from the initially elevated Li^+ concentration in the solution, which maintains a Li^+-rich surface on the thick electrode during the reaction, thus increasing capacity. Notably, there was no significant difference in capacity between the two electrodes at 200 ppm and 500 ppm. (S-PVDF: 37.57 mg·g^{-1} vs. 38.53 mg·g^{-1}, PVDF: 30.67 mg·g^{-1} vs. 31.79 mg·g^{-1}), indicating good adaptability at 200 ppm. Additionally, the S-PVDF thick electrode demonstrated higher capacity than the traditional thick electrode above 200 ppm (with an efficiency of approximately 88.1 % in Fig. 4d). This may be because the introduction of sulfonic acid groups enhances the hydrophilicity of the electrode, thereby improving the utilization of active materials.

The Li^+ extraction efficacy of the thick electrode with S-PVDF binder was assessed using simulated and actual West Taijinar old brine. The CV curve of the S-PVDF thick electrode in simulated West Taijinar brine shows three oxidation peaks (0.06 V, 0.1 V, 0.19 V) and two reduction peaks (0.27 V, 0.04 V) (Fig. 4e and Table S2a). In general, Na^+ has two oxidation peaks and one reduction peak, Li^+ has one reduction peak of the oxidation class, and the two oxidation peaks and reduction peaks of Na^+ are at the left of the corresponding peaks of Li^+ [26]. Hence, 0.06 V, 0.1 V, and 0.27 V are the characteristic peaks of Na^+ CV curve, and 0.19 V and 0.04 V are the characteristic peaks of Li^+. The intercalation of Na^+ in S-PVDF thick electrode was demonstrated during testing with simulated brine. A lithium extraction test was conducted (Fig. 4f). The average Li^+ capacity can reach 29.34 mg·g^{-1}, and the Na^+/Li^+ ratio decreases from 55 to 0.55 after 5 cycles (Fig. S6), indicating that a small part of Na^+ is intercalated in the S-PVDF thick electrode. This is consistent with the CV curve. This phenomenon contributes leads to the reduced capacity of S-PVDF thick electrodes compared to those operating in a purely lithium-based environment. However, only the Li^+ intercalation peak appeared in the CV curve when using old West Taijinar brine as the electrolyte. The test with old West Taijinar brine was conducted (Table S2b). In practical applications, the S-PVDF thick electrode exhibits a commendable Li^+ extraction capacity, averaging 28.8 mg·g^{-1} over 5 cycles (Fig. 4h), achieving a satisfactory separation of Na^+, Mg^{2+} and Li^+. After 5 cycles, the Na^+/Li^+ ratio in the recovered solution decreased to 0.16 (Fig. S7). The Mg^{2+}/Li^+ ratio was reduced from 65.6 to 0.37 after 5 cycles (Fig. 4i). Sulfonate facilitates the effective separation of Mg^{2+} and Li^+. Under the influence of an electric field, both Mg^{2+} and Li^+ move toward $FePO_4$ particles. As the ions diffuse to the surface of $FePO_4$ particles coated with S-PVDF, the interaction between Mg^{2+} and the sulfonic acid group is stronger than that with Li^+. This is because the negatively charged sulfonic acid group has a stronger attraction to higher-charge ions like Mg^{2+} [27,28]. Consequently, most Mg^{2+} is drawn to S-PVDF, while $FePO_4$ selectively interacts with Li^+ at a specific potential, driving Li^+ into the lattice and increasing overall selectivity [29]. This indicates that enhancing the infiltrability of the S-PVDF thick electrode increases the utilization rate of active substances and effectively improves Li^+ intercalating ability and selectivity.

Furthermore, Energy consumption is extracted once by S-PVDF electrode and deintercalation Li^+ is calculated at 0.8 V. The relationship between time and current is shown in Fig. S8. It can be seen that the current in the simulated brine decreases faster than that in the actual old brine. Meanwhile, the lithium extraction capacity of S-PVDF in the simulated brine is higher, indicating that the embedding kinetics of Li^+ in the simulated brine is faster and it is easier to intercalated the electrode. This is because the actual old brine environment is complex, the ion concentration is larger and the viscosity is higher, and the Li^+ moves slowly. In addition, the energy consumption of S-PVDF electrode in simulated brine and actual brine was calculated according to Eq. (1). The calculated values are 3.9 Wh·mol^{-1} and 4.53 Wh·mol^{-1} respectively, which once again verifies that Li^+ moves slowly in the actual brine and requires greater energy consumption to embed the electrode. In addition, it can be seen from Fig. 4h and f that the simulated brine efficiency and the actual brine efficiency are 64.4 % and 59 % respectively. The S-PVDF electrode has higher capacity in simulated brine, easier to embed electrode and lower energy consumption.

$$E_{sec} = \frac{M_{Li} \cdot U \cdot \int_0^t I(t)dt}{3.6 E_{Li} \cdot w} \quad (1)$$

where E_{sec} is specific energy consumption [Wh·mol^{-1}]; M_{Li} Is the molar mass of Li [6.941 g·mol^{-1}]; U is the applied voltage in the process of external voltage driving [V]; I is the current [A] value; t is the operation time [s]; E_{Li} is the extraction amount of Li [mg·g^{-1}]; W is the mass of LFP [g].

3.5. Physical characteristics and simulation of thick electrode

Fig. 5a displays the contact angles of the two electrodes in both water and brine. The S-PVDF electrode consistently demonstrates higher hydrophilicity compared to the PVDF electrode in both environments. Specifically, when in contact with water, the S-PVDF electrode exhibits a significantly lower contact angle (43° vs. 106° / Fig. 4a upper left and lower left). At the same time, the S-PVDF electrode still showed good hydrophilicity (70° Vs 125° /Fig. 4a upper right and lower right) when tested with the brine at the contact angle. Compared with water, the contact angle is obviously increased, because the brine itself has high viscosity and high calcification, which makes the infiltration decrease. Additionally, when water was injected into the blended vial (without stirring), the S-PVDF slurry dispersed evenly in the petri dish, whereas the PVDF slurry agglomerated. This may be due to the hydrophobic nature of PVDF, which causes the NMP solvent in the PVDF adhesive to diffuse into water upon contact. This increases the concentration of PVDF adhesive near the aqueous phase, leading to phase separation and curing [30]. Consequently, electrodes with S-PVDF binders demonstrate superior surface wettability compared to those with PVDF binders.

Finite element simulation was employed to verify the infiltration effect of the 45 mg·cm^{-2} thick S-PVDF electrode in brine. Fig. 5c and d compares the infiltration effects of S-PVDF and PVDF electrodes using COMSOL Multiphysics 5.5 simulations over 60 s. The numerical simulations reveal that the S-PVDF electrode achieves 100 % infiltrability within 60 s, significantly outperforming the PVDF electrode, which only reaches 70 %. Theoretical simulations indicate that the infiltrability of the S-PVDF electrode with brine is excellent, facilitating even distribution within the electrode and effectively increasing the electrochemical reaction surface area. This is consistent with the conclusion of contact angle between electrodes and different solutions. Experimental and theoretical results show that S-PVDF has good hydrophilicity. Additionally, good wettability typically leads to a stable electrode-brine interface, reducing polarization and interface impedance in the electrolyte. This stability enhances the efficiency of the electrochemical reaction, thereby boosting the Li^+ extraction capacity of the high-load S-PVDF electrode [31]. Furthermore, Fig. 5e illustrates the hydrophilic mechanism of the S-PVDF thick electrode. Water molecules, acting as a conducting medium, form extended hydrogen bonds within the electrode's sulfonic acid-lined pores. The oxygen atom in the sulfonic acid group carries a negative charge and electrostatically interacts with some of the positively charged hydrogen atoms in water molecules. This charge interaction enhances the attraction between the sulfonic acid group and water molecules [32]. In addition, Based on the Young-Dupre equation (Eq. (S1)), the formation of hydrogen bond reduces the interface energy between the electrode material and the liquid electrolyte from the perspective of thermodynamics. As a result, the brine can effectively infiltrate the electrode, promoting the initial adsorption of brine on the electrode surface, The network of hydrogen bonds formed acts as an ion transport pathway, leading to the efficient transmission of Li^+ [33–35]. This enhances the electrode-brine contact, thereby

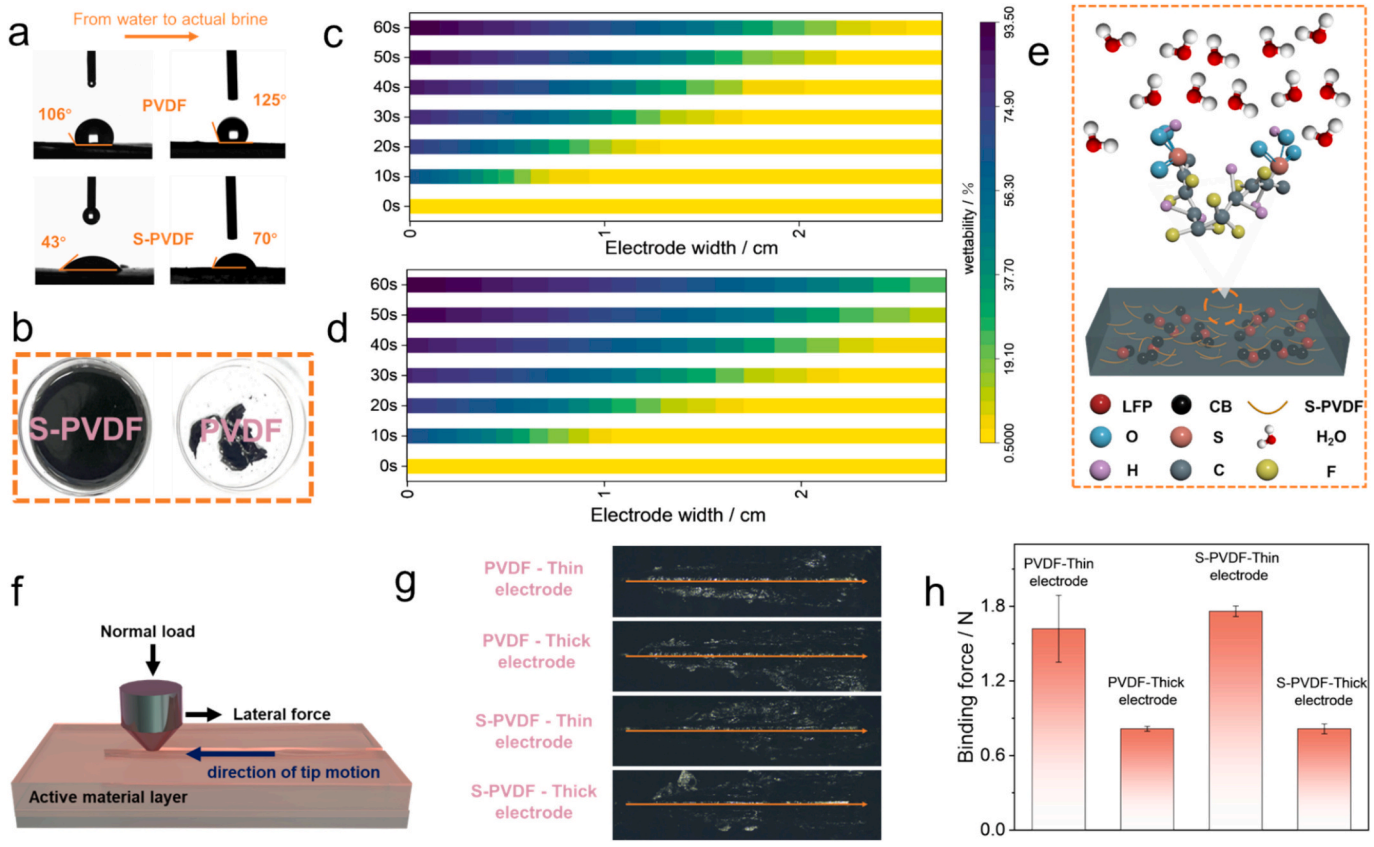

Fig. 5. Physical characteristics and simulation of thick electrode. (a) Contact angle of S-PVDF and PVDF electrode water and brine. (b) The electronic image after adjusting the slurry and adding water. (c) and (d) Simulation of PVDF and S-PVDF thick electrode infiltration. (e) Diagram of S-PVDF hydrophilic mechanism. (f) Schematic diagram of the nanoscratch. (g) Nanoscratch physical electronic picture. (h) The binding force of PVDF and S-PVDF electrodes with different load capacities.

boosting the electrode's lithium extraction efficiency. Simultaneously, the formation of hydrogen bond networks can immobilize water molecules, thereby suppressing hydrogen evolution and preventing side reactions induced by brine [35].

The binding force between the adhesive and fluid collector before and after sulfonation was determined by nanoscratch test. The test principle of nanoscratch experiment is shown in Fig. 5f. Upon evaluating the binding force, a detailed representation of the scratch patterns can be observed in Fig. 5g. There is little difference between the binding force of PVDF electrode loaded with 3 $mg{\cdot}cm^{-2}$ or 7 $mg{\cdot}cm^{-2}$ and S-PVDF electrode (Fig. 5h). This indicates that properly sulfonated PVDF not only ensures the wettability of the electrode and brine, but also maintains its viscosity.

3.6. Comparison of this work with other methods

This paper presents a comparative analysis of the performance of thick electrodes, as shown in Table S3, with a focus on capacity, load, and brine composition. Works 1 and 2 achieved capacities of 23.87 $mg{\cdot}g^{-1}$ and 24.9 $mg{\cdot}g^{-1}$, respectively, in real brine using three-dimensional thick electrodes (20 $mg{\cdot}cm^{-2}$). In contrast, our study employed electrodes with a load of up to 45 $mg{\cdot}cm^{-2}$, resulting in a higher capacity of 28.8 $mg{\cdot}g^{-1}$. Thus, our electrodes outperform the three-dimensional thick electrodes under increased load conditions. Additionally, Works 3 and 4 achieved electrode loads of up to 85 $mg{\cdot}cm^{-2}$ in real brine, with capacities of 15 $mg{\cdot}g^{-1}$ and 27.3 $mg{\cdot}g^{-1}$, respectively. Although Work 4 achieved a capacity similar to ours under high loads, the brine used in Work 4 had a significantly higher Li^+ concentration of 1.84 $g{\cdot}L^{-1}$, compared to only 0.711 $g{\cdot}L^{-1}$ in our study. The Li^+ concentration is affected by the climatic conditions of the salt pan, resulting in substantial Li^+ loss and longer processing times. Thus, our approach is better suited for lower brine concentrations, minimizing both time and Li+ losses. As shown in the table, S-PVDF thick electrodes exhibit clear benefits, providing high capacity and efficient separation, even in challenging environments.

4. Conclusion

In conclusion, this work proves that controlling the hydrophilicity of thick electrodes is the key to increase the intercalation Li^+ capacity. During operation, the S-PVDF electrode's sulfonic groups form hydrogen bonds with water, improving the electrode's wettability and active material utilization. Experiments and simulations confirm the S-PVDF electrode's superior brine infiltration and stable intercalation capacity (28.8 $mg{\cdot}g^{-1}$). The Mg^{2+}/Li^+ ratio significantly decreased from 65 to 0.37, efficiently achieving Mg-Li separation. This research advances lithium extraction via electrochemical de-lithiation, offering valuable insights for its practical application.

Declaration of competing interest

We declare no commercial or associative interests that pose a conflict of interest with the work submitted.

Acknowledgments

This research received funding from the Haixi Science and Technology Planning Project, under Grant No. 2024-JC-Q01.

Appendix A. Supplementary data

Supplementary data to this article can be found online at https://doi.org/10.1016/j.desal.2025.118669.

Data availability

The data that has been used is confidential.

References

[1] G. Yihong, Y. Jianguo, S. Haiping, Desorption enhancement of aluminum-based adsorbent in lithium extraction from sulfate-type salt lakes, Desalination 571 (2024) 117113.

[2] D. Mingzhe, L. Qinglong, S. Kaiyuan, W. Zhijian, T. Jie, Reconstruction of MgAl-layered double hydroxides to LiAl-layered double hydroxides for scalable lithium extraction from salt lake brine, Miner. Eng. 202 (2023) 108293.

[3] J. Zhang, Z. Cheng, X. Qin, X. Gao, M. Wang, X. Xiang, Recent advances in lithium extraction from salt lake brine using coupled and tandem technologies, Desalination 547 (2023).

[4] M. Awais Ashraf, M. Usman, I. Hussain, F. Ahmad, S. Guo, L. Zhang, Lithium extraction from high magnesium salt lake brine with an integrated membrane technology, Separ. Purif. Technol. 302 (2022) 122163.

[5] L. Chong, L. Yanbin, L. Dingchang, H. Po-Chun, L. Bofei, Y. Gangbin, W. Tong, C. Yi, C. Steven, Lithium extraction from seawater through pulsed electrochemical intercalation, Joule 4 (2020) 1459–1469.

[6] G. Jun, C. Linlin, Z. Wenshuai, Multifunctional $AlPO_4$ reconstructed $LiMn_2O_4$ surface for electrochemical lithium extraction from brine, journal of energy, Chemistry 89 (2023) 410–421.

[7] Z.Y.Z.Y.C.W.X.Z.L.W.Y.Y.X.S.D.S.H.Y.C. Yanxi Yu, Thermally assisted efficient electrochemical lithium extraction from simulated seawater, Water Res. 223 (2022) 118969.

[8] C. Ying, Z. Honglong, Q. Yingjun, Facet dependent ion channel of iron phosphate for electrochemical lithium extraction, Chem. Eng. J. 477 (2023) 147136.

[9] W. Xu, L. He, Z. Zhao, Lithium extraction from high Mg/Li brine via electrochemical intercalation/de-intercalation system using $LiMn_2O_4$ materials, Desalination 503 (2021) 114935.

[10] Z. Zhao, X. Si, X. Liu, L. He, X.J.H. Liang, Li extraction from High Mg/Li Ratio Brine with $LiFePO_4/FePO_4$ as Electrode Materials 133, 2013, pp. 75–83.

[11] J. Xiong, L. He, Z.J.D. Zhao, Lithium extraction from high-sodium raw brine with $Li_{0.3}FePO_4$ electrode 535 (2022) 115822.

[12] J. Lee, H. Lee, C. Bak, Y. Hong, D. Joung, J.B. Ko, Y.M. Lee, C.J.N.-M.L. Kim, Enhancing hydrophilicity of thick electrodes for high energy density aqueous batteries 15 (2023) 97.

[13] Q. Wang, F. Jia, S. Song, Y. Li, Hydrophilic MoS_2/polydopamine (PDA) nanocomposites as the electrode for enhanced capacitive deionization, Sep. Purif. Technol. 236 (2020), 116298.

[14] K. Tang, Z. Li, Y. Da Wang, J. McClure, H. Su, P. Mostaghimi, R.T. Armstrong, A pore-scale model for electrokinetic in situ recovery of copper: the influence of mineral occurrence, zeta potential, and electric potential, Transp. Porous Media 150 (2023), 601-626.

[15] K. Tang, Z. Bo, Z. Li, Y. Da Wang, J. McClure, H. Su, P. Mostaghimi, R.T.J.P.O. F. Armstrong, Controlled ion transport in the subsurface: a coupled advection–diffusion–electromigration system 36 (2024).

[16] H. Su, K.A.S. Usman, A. Nilghaz, Y. Bu, K. Tang, L. Dai, D. Liu, J.M. Razal, W. Lei, J. J.D. Tian, Efficient energy generation from a sweat-powered, wearable, MXene-based hydroelectric nanogenerator 2 (2024).

[17] T. Vo Dinh Cong, C. Bhandari Subash, B. Anima, A sulfonated polydopamine coated-PVDF membrane development for oil/water separation via eco-friendly methodology, journal of environmental, Chem. Eng. 11 (2023) 110560.

[18] W. Zhilu, F. Guoying, Y. Zhiguo, L. Shaopin, X. Man, W. Cunwen, L. Yanbo, Improving the hydrophilicity and antifouling performance of PVDF membranes via PEI amination and further poly (methyl vinyl ether-alt-maleic anhydride) modification, React. Funct. Polym. 189 (2023) 105610.

[19] L. Jian, H. Hongying, Y. Xiaohua, R. Ju, C. Fangshu, Building the homogeneous ionic interfaces and channels for high compatible composite PVDF/SiO_2 solid electrolyte by grafting sulfonate betaine, Surf. Interfaces 39 (2023) 102978.

[20] H. Farrokhzad, T. Kikhavani, F. Monnaie, S.N. Ashrafizadeh, G. Koeckelberghs, T. Van Gerven, B. Van der Bruggen, Novel composite cation exchange films based on sulfonated PVDF for electromembrane separations, J. Membr. Sci. 474 (2015) 167–174.

[21] M. Amélie, F. Kateryna, T. Lina, D. Adam, O. Hassan, Sulfonation of polyvinylidene fluoride: investigation of the microstructure by {1H, 13C, 19F} NMR spectroscopy and mechanisms, ACS Appl. Polym. Mater. 4 (2022) 9463–9471.

[22] J. Ren, W. Xia, X. Feng, Y. Zhao, Surface modification of PVDF membrane by sulfonated chitosan for enhanced anti-fouling property via PDA coating layer, Mater. Lett. 307 (2022) 130981.

[23] X. Weimin, Z. Zhicheng, PVDF-based dielectric polymers and their applications in electronic materials, IET Nanodielectrics 1 (2018) 17–31.

[24] R. Guan, H. Zou, D.P. Lu, C.L. Gong, Y.F. Liu, Polyethersulfone sulfonated by chlorosulfonic acid and its membrane characteristics, Eur. Polym. J. 41 (2005) 1554–1560.

[25] L. Jiaxu, R. Junfeng, L. Caixia, L. Pengxian, W. Tingting, L. Shiwei, W. Lei, High-adhesion anionic copolymer as solid-state electrolyte for dendrite-free Zn-ion battery, Nano Res. 15 (2022) 7190–7198.

[26] J. Xiong, L. He, D. Liu, W. Xu, Z. Zhao, Olivine-$FePO_4$ preparation for lithium extraction from brines via electrochemical de-intercalation/intercalation method, Desalination 520 (2021) 115326.

[27] Z. Lu, Y. Wu, L. Ding, Y. Wei, H.J.A.C. Wang, A lamellar MXene ($Ti_3C_2T_x$)/PSS composite membrane for fast and selective lithium-ion separation 133 (2021) 22439–22443.

[28] S. Liu, X. Tong, L. Huang, C. Xiao, K. Zhang, Y. Chen, J.J.J.O.M.S. Crittenden, Lithium-ion extraction using electro-driven freestanding graphene oxide composite membranes 672 (2023) 121448.

[29] H. Yu, M.J. Park, C. Wang, D. Liang, T. He, G. Naidu, D.S. Han, H.K.J.S. Shon, P. Technology, Integrated sulfonated poly ether ketone membrane capacitive deionization for lithium recovery from diluted binary solutions 352 (2025) 128064.

[30] A. Sivasankaran, A. Young-Ho, Fabrication and application of novel high strength sulfonated PVDF ultrafiltration membrane for production of reclamation water, Chemosphere 305 (2022) 135416.

[31] L. Zhao, Y. Li, M. Yu, Y. Peng, F.J.A.S. Ran, Electrolyte-wettability issues and challenges of electrode materials in electrochemical energy storage, energy conversion, and beyond 10 (2023) 2300283.

[32] D.K. Maity, K. Otake, S. Ghosh, H. Kitagawa, D. Ghoshal, Sulfonic group functionalized mixed ligand coordination polymers: synthesis, characterization, water sorption, and proton conduction studies, Inorg. Chem. 56 (2017), 1581-1590.

[33] X. Kun, S. Yiqiang, L. Xiuling, Z. Zihan, Z. Yongqi, L. Cuncheng, F. Hong Jin, Fluorine-induced dual defects in cobalt phosphide Nanosheets enhance hydrogen evolution reaction activity, ACS, Mater. Lett. 2 (2020) 736–743.

[34] Y.L.M.Y.Y.P.F.R. Lei Zhao, Electrolyte-wettability issues and challenges of electrode materials in electrochemical energy storage, energy conversion, and beyond, advanced science (Weinheim, Baden-Wurttemberg, Germany) 10 (2023) e2300283.

[35] P. Wang, S. Liang, C. Chen, X. Xie, J. Chen, Z. Liu, Y. Tang, B. Lu, J. Zhou, Spontaneous construction of nucleophilic carbonyl-containing interphase toward ultrastable zinc-metal anodes, Adv. Mater. 34 (2022) e2202733.